

# Peak-structure in self-energy of cuprate superconductors

Yiqun Liu<sup>1\*</sup>, Yu Lan<sup>2\*</sup>, and Shiping Feng<sup>1†</sup>

<sup>1</sup>*Department of Physics, Beijing Normal University, Beijing 100875, China and*

<sup>2</sup>*College of Physics and Electronic Engineering, Hengyang Normal University, Hengyang 421002, China*

The recently deduced normal and anomalous self-energies from photoemission spectra of cuprate superconductors via machine learning are calling for an explanation. Here the normal and anomalous self-energies in cuprate superconductors are analyzed within the framework of the kinetic-energy-driven superconductivity. It is shown that the exchanged spin excitations give rise to the well-pronounced peak-structures in both the normal and anomalous self-energies at all around the electron Fermi surface except for at the hot spots, where the peak-structures are absent. In particular, the peak-structure in the normal self-energy is mainly responsible for the peak-dip-hump structure in the single-particle excitation spectrum, and can persist into the normal-state, while the sharp peak in the anomalous self-energy gives rise to a crucial contribution to the superconducting gap, and vanishes in the normal-state. Moreover, the evolution of the peak-structure with doping and momentum are also analyzed.

PACS numbers: 74.25.Jb, 74.20.Mn, 74.72.-h

The strong electron correlation is foundational to the emergence of superconductivity in cuprate superconductors<sup>1,2</sup>, where the strong interaction of the electrons with collective bosonic excitations of different origins results in (i) the energy and lifetime renormalization of the electrons in the particle-hole channel to form the quasiparticles responsible for the anomalous properties, and (ii) the formation of the electron pairs in the particle-particle channel responsible for superconductivity below the superconducting (SC) transition temperature  $T_c$ . This is why the quasiparticles in the SC-state determined by the electronic structure is intimately related to the pairing glue forming electron pairs<sup>3-7</sup>. In conventional superconductors, the renormalization of the electrons in the particle-hole channel and the formation of the electron pairs in the particle-particle channel are caused by the interaction between the electrons by the exchange of phonons<sup>8-10</sup>. Although a significant effort has been made for the past three decades, what type of the collective bosonic excitation that can mediate electron pairing in cuprate superconductors in analogy to the phonon-mediate pairing mechanism in conventional superconductors is still debated<sup>2-7</sup>.

Angle-resolved photoemission spectroscopy (ARPES) is a direct tool to probe the energy and momentum of quasiparticles simultaneously<sup>3-5</sup>, where a quasiparticle with a long lifetime is observed as a sharp peak in intensity, and a quasiparticle with a short lifetime is observed as a broad peak. However, the energy and lifetime of the quasiparticle in the SC-state are directly described by the real and imaginary parts of the total self-energy<sup>3-7</sup>  $\text{Re}\Sigma_{\text{tot}}(\mathbf{k}, \omega)$  and  $\text{Im}\Sigma_{\text{tot}}(\mathbf{k}, \omega)$ , respectively. This total self-energy  $\Sigma_{\text{tot}}(\mathbf{k}, \omega)$  is a specific combination of the normal self-energy  $\Sigma_{\text{ph}}(\mathbf{k}, \omega)$  in the particle-hole

channel and the anomalous self-energy  $\Sigma_{\text{pp}}(\mathbf{k}, \omega)$  in the particle-particle channel<sup>9-12</sup>. In other words, only the total self-energy can be extracted directly from ARPES experiments, and the only ingredient that needs to extract the total self-energy is the quasiparticle spectral density observed by ARPES experiments<sup>3-5</sup>. However, for our exploration of the bosonic mode coupling that is how electron self-energy effects appeared in our theoretical analysis, it is crucial to extract the normal and the anomalous self-energies separately<sup>9-12</sup>. This follows a basic fact that although both the normal and anomalous self-energies are generated by the same electron interaction mediated by collective bosonic excitations, they describe theoretically different parts of the interaction effects. The normal self-energy  $\Sigma_{\text{ph}}(\mathbf{k}, \omega)$  describes the single-particle coherence, and therefore competes with superconductivity. Moreover, it gives rise to a main contribution to the energy and lifetime renormalization of the electrons, and then all the anomalous properties of cuprate superconductors arise from this renormalization of the electrons<sup>13-16</sup>. On the other hand, the SC-state is characterized by the anomalous self-energy  $\Sigma_{\text{pp}}(\mathbf{k}, \omega)$ , which is identified as the energy and momentum dependent SC gap in the single-particle excitation spectrum, and therefore is corresponding to the energy for breaking an electron pair<sup>9-12</sup>. In this case, if both the normal and anomalous self-energies are deduced from the experimental data, it can be used to examine a microscopic SC theory and understand the details of the SC-state.

Although both the normal and anomalous self-energies can not be measured directly from the ARPES experiments, the Boltzmann-machine learning technique has been applied recently to deduce both the normal and anomalous self-energies from the experimental data of the ARPES spectra observed in  $\text{Bi}_2\text{Sr}_2\text{CaCu}_2\text{O}_{8+\delta}$  at the optimum doping and  $\text{Bi}_2\text{Sr}_2\text{CuO}_{6+\delta}$  in the underdoped regime<sup>17</sup>, and the deduced results show clearly that both the normal and anomalous self-energies exhibit the no-

<sup>†</sup>E-mail address: spfeng@bnu.edu.cn

\* These authors contributed equally to this work

table peak-structures, however, these peak-structures do not appear in the total self-energy. In particular, the peak in the anomalous self-energy makes a dominant contribution to the SC gap, and therefore provide a decisive testimony for the origin of superconductivity<sup>17</sup>. These normal and anomalous self-energies of cuprate superconductors revealed by the machine learning approach therefore are calling for a systematic analysis. Quite recently, these deduced normal and anomalous self-energies in Ref. 17 have been analyzed within an effective fermion-boson theory<sup>18</sup>, and the result indicates that the pairing electrons is mediated by a soft, near-critical bosonic mode. In particular, this analysis also shows that if the sharp peaks in both the normal and anomalous self-energies survive down to the lowest temperatures, their presence alone imposes the strong restrictions on the energy dependence of a soft pairing boson<sup>18</sup>. However, the full understanding of these peak-structures in both normal and anomalous self-energies is still open for further analyses. In this paper, we make a comparison of the deduced normal and anomalous self-energies in Ref. 17 with those obtained based on the kinetic-energy driven SC mechanism<sup>19–22</sup>, and then show explicitly that the interaction between electrons by the exchange of spin excitations generates the well-pronounced peak-structures in both the normal and anomalous self-energies at all around the electron Fermi surface (EFS) except for at around the hot spots, where the peak-structures are absent, in qualitative agreement with the corresponding results in the normal and anomalous self-energies deduced via machine learning<sup>17</sup>. In particular, we show clearly that the peak-structure in the normal self-energy is mainly responsible for the famous peak-dip-hump (PDH) structure in the single-particle excitation spectrum<sup>23–27</sup>, and can persist into the normal-state, while the sharp peak in the anomalous self-energy gives rise to a crucial contribution to the SC gap, and vanish in the normal-state. More specifically, the peak-structures in both the normal and anomalous self-energies are doping dependent, where in the underdoped regime, the position of the peak in the anomalous self-energy at around the antinode moves to higher energies with the increase of doping, while the peak in the normal self-energy at around the  $[\pi, 0]$  point of the Brillouin zone (BZ) moves to lower energies. Furthermore, the peak-structures also have a striking momentum dependence, with the position of the peak in the normal self-energy that shifts to lower energies when one moves the momentum from the antinode to the node.

The following analyses of the normal and anomalous self-energies in cuprate superconductors build on the kinetic-energy driven superconductivity<sup>19–22</sup>, which was established early based on the  $t$ - $J$  model in the charge-spin separation fermion-spin representation. In this kinetic-energy driven SC mechanism, the interaction between the charge carriers directly from the kinetic energy of the  $t$ - $J$  model by the exchange of *spin excitations* is responsible for the d-wave charge-carrier pairing in the particle-particle channel, then the d-wave electron pairs

originated from the d-wave charge-carrier pairing state are due to the charge-spin recombination, and their condensation reveals the d-wave SC-state. Moreover, the renormalization of the electrons in cuprate superconductors has been investigated recently within the framework of the kinetic-energy driven superconductivity<sup>28–30</sup>, and then the main features of the single-particle excitation spectrum are well reproduced. In these previous works<sup>22</sup>, the single-particle diagonal and off-diagonal propagators of the  $t$ - $J$  model in the SC-state have been obtained in terms of the full charge-spin recombination, and can be expressed explicitly as,

$$G(\mathbf{k}, \omega) = \frac{1}{\omega - \varepsilon_{\mathbf{k}} - \Sigma_{\text{tot}}(\mathbf{k}, \omega)}, \quad (1a)$$

$$\mathcal{G}^\dagger(\mathbf{k}, \omega) = \frac{L_{\mathbf{k}}(\omega)}{\omega - \varepsilon_{\mathbf{k}} - \Sigma_{\text{tot}}(\mathbf{k}, \omega)}, \quad (1b)$$

where the single-electron band energy  $\varepsilon_{\mathbf{k}} = -4t\gamma_{\mathbf{k}} + 4t'\gamma'_{\mathbf{k}} + \mu$ , with  $\gamma_{\mathbf{k}} = (\cos k_x + \cos k_y)/2$ ,  $\gamma'_{\mathbf{k}} = \cos k_x \cos k_y$ , and the chemical potential  $\mu$ ,  $L_{\mathbf{k}}(\omega) = -\Sigma_{\text{pp}}(\mathbf{k}, \omega)/[\omega + \varepsilon_{\mathbf{k}} + \Sigma_{\text{ph}}(\mathbf{k}, -\omega)]$ , while the total self-energy  $\Sigma_{\text{tot}}(\mathbf{k}, \omega)$  is a well-known combination of the normal self-energy  $\Sigma_{\text{ph}}(\mathbf{k}, \omega)$  and the anomalous self-energy  $\Sigma_{\text{pp}}(\mathbf{k}, \omega)$  as,

$$\Sigma_{\text{tot}}(\mathbf{k}, \omega) = \Sigma_{\text{ph}}(\mathbf{k}, \omega) + W_{\mathbf{k}}(\omega), \quad (2)$$

with the additional contribution  $W_{\mathbf{k}}(\omega)$  below  $T_c$  due to the SC gap opening,

$$W_{\mathbf{k}}(\omega) = \frac{|\Sigma_{\text{pp}}(\mathbf{k}, \omega)|^2}{\omega + \varepsilon_{\mathbf{k}} + \Sigma_{\text{ph}}(\mathbf{k}, -\omega)}. \quad (3)$$

In the framework of the kinetic-energy driven superconductivity, both the normal and anomalous self-energies  $\Sigma_{\text{ph}}(\mathbf{k}, \omega)$  and  $\Sigma_{\text{pp}}(\mathbf{k}, \omega)$  arise from the interaction between electrons mediated by spin excitations, and have been given explicitly in Ref. 22.

The single-particle spectral function  $A(\mathbf{k}, \omega)$  measured by ARPES experiments is related directly to the imaginary part of the single-particle diagonal propagator in Eq. (1a) as<sup>3–5</sup>,

$$A(\mathbf{k}, \omega) = \frac{-2\text{Im}\Sigma_{\text{tot}}(\mathbf{k}, \omega)}{[\omega - \varepsilon_{\mathbf{k}} - \text{Re}\Sigma_{\text{tot}}(\mathbf{k}, \omega)]^2 + [\text{Im}\Sigma_{\text{tot}}(\mathbf{k}, \omega)]^2}, \quad (4)$$

where  $\text{Re}\Sigma_{\text{tot}}(\mathbf{k}, \omega)$  and  $\text{Im}\Sigma_{\text{tot}}(\mathbf{k}, \omega)$  are the real and imaginary parts of the total self-energy  $\Sigma_{\text{tot}}(\mathbf{k}, \omega)$ , respectively. In ARPES experiments<sup>3–5</sup>, the energy renormalization of the electrons in cuprate superconductors is directly determined by the real part of the total self-energy, while the lifetime renormalization of the electrons is completely governed by the imaginary part of the total self-energy. This is also why only the total self-energy can be extracted directly from ARPES experiments. In the following discussions, the parameters in the  $t$ - $J$  model are chosen as  $t/J = 3.5$  and  $t'/t = 0.4$ . However, when necessary to compare with the experimental data, we take  $J = 100$  meV, which is the typical value of cuprate superconductors<sup>3–5</sup>.

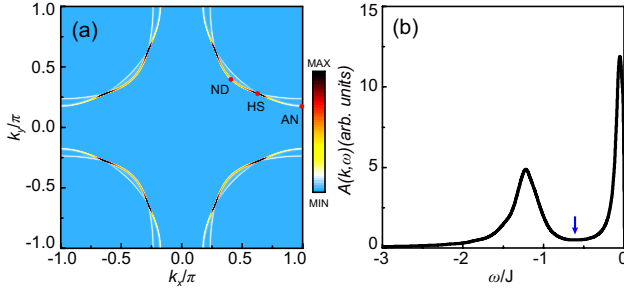


FIG. 1: (Color online) (a) The electron Fermi surface map and (b) the single-particle excitation spectrum at the antinode as a function of energy in  $\delta = 0.15$  with  $T = 0.002J$  for  $t/J = 3.5$  and  $t'/t = 0.4$ , where AN, HS, and ND in (a) denote the antinode, hot spot, and node, respectively, while the blue arrow in (b) indicates the position of the dip.

In an interacting electron system, the topology of EFS plays a crucial role in the understanding of the physical properties, since everything happens at EFS. In particular, the strong coupling between the electrons and spin excitations in cuprate superconductors leads to a strong redistribution of the spectral weights on EFS<sup>28–30</sup>, which cause the normal and anomalous self-energies to strongly vary with the Fermi angle around EFS. For a convenience in the following discussions, (a) the underlying EFS map<sup>28</sup> and (b) the single-particle excitation spectrum<sup>28,29</sup>  $A(\mathbf{k}_{\text{AN}}, \omega)$  at the antinode as a function of energy for doping  $\delta = 0.15$  with temperature  $T = 0.002J$  are replotted in Fig. 1. The result in Fig. 1a therefore shows that EFS has been separated into three characteristic regions due to the strong redistribution of the spectral weight: (a) the antinodal region, where the spectral weight is suppressed, leading to that EFS around the antinodal region becomes unobservable in experiments<sup>31–34</sup>; (b) the nodal region, where the spectral weight is reduced modestly, leading to that EFS is truncated to form the disconnected Fermi arcs located around the nodal region<sup>31–34</sup>; (c) the hot spot region, where the renormalization from the quasiparticle scattering further reduces almost all spectral weight on Fermi arcs to the tips of the Fermi arcs<sup>35–38</sup>. In this case, the spectral intensity exhibits a largest value at around the tips of the Fermi arcs, and only in this sense, these tips of the Fermi arcs are called as the hot spots on EFS. Moreover, these hot spots connected by the scattering wave vectors  $\mathbf{q}_i$  construct an *octet* scattering model, which is a basic scattering model in the explanation of the Fourier transform scanning tunneling spectroscopy experimental data, and also can give a consistent description of the regions of the highest joint density of states detected from ARPES autocorrelation experiments<sup>30,36</sup>. On the other hand, the result in Fig. 1b indicates that the characteristic feature in the single-particle excitation spectrum is the dramatic change in the spectral line-shape<sup>23–27</sup>, where a quasiparticle peak develops at the lowest energy, followed by a dip and a hump, giving rise to the strik-

ing PDH structure. All these theoretical results are well consistent with the corresponding results observed from the ARPES experiments.

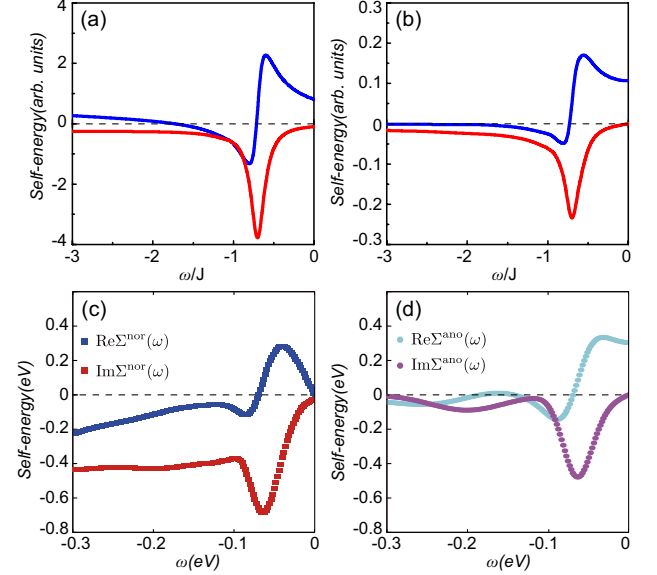


FIG. 2: (Color online) (a) The real (blue line) and imaginary (red line) parts of the normal self-energy and (b) the real (blue line) and imaginary (red line) parts of the anomalous self-energy at the antinode as a function of energy in  $\delta = 0.15$  with  $T = 0.002J$  for  $t/J = 3.5$  and  $t'/t = 0.4$ . The corresponding results of (c) the real and imaginary parts of the normal self-energy and (d) the real and imaginary parts of the anomalous self-energy around the antinode as a function of energy deduced from the ARPES spectra of the optimally doped  $\text{Bi}_2\text{Sr}_2\text{CaCu}_2\text{O}_{8+\delta}$  via machine learning taken from Ref. 17.

We are now ready to analyze the doping and momentum dependence of the normal and anomalous self-energies in cuprate superconductors. In Fig. 2, we plot (a) the real (blue line) and imaginary (red line) parts of the normal self-energy and (b) the real (blue line) and imaginary (red line) parts of the anomalous self-energy at the antinode as a function of energy for  $\delta = 0.15$  with  $T = 0.002J$ . For a better comparison, the corresponding results<sup>17</sup> of (c) the real and imaginary parts of the normal self-energy and (d) the real and imaginary parts of the anomalous self-energy around the antinode as a function of energy deduced from the ARPES spectra of the optimally doped  $\text{Bi}_2\text{Sr}_2\text{CaCu}_2\text{O}_{8+\delta}$  via machine learning are also shown in Fig. 2. Apparently, the main features of both the normal and anomalous self-energies deduced via machine learning<sup>17</sup> are well reproduced, where all the real and imaginary parts of the normal and anomalous self-energies exhibit the remarkable peak-structures. Since the strength of the electron pair is directly determined by the anomalous self-energy, these peaks in both  $\text{Re}\Sigma_{\text{pp}}(\mathbf{k}_{\text{AN}}, \omega)$  and  $\text{Im}\Sigma_{\text{pp}}(\mathbf{k}_{\text{AN}}, \omega)$  give rise to a crucial contribution to the SC gap, and therefore are the true origin of the high  $T_c$  in cuprate superconductors<sup>17</sup>. On

the other hand, since the single-particle coherence is associated directly with the normal self-energy, these peaks in  $\text{Re}\Sigma_{\text{ph}}(\mathbf{k}_{\text{AN}}, \omega)$  and  $\text{Im}\Sigma_{\text{ph}}(\mathbf{k}_{\text{AN}}, \omega)$  dominate the energy and lifetime renormalization of the electrons, respectively. In particular, the sharp peak in  $\text{Im}\Sigma_{\text{pp}}(\mathbf{k}_{\text{AN}}, \omega)$  locates at the same energy  $\omega_{\text{Im-Th}} \sim -70$  meV as that in  $\text{Im}\Sigma_{\text{ph}}(\mathbf{k}_{\text{AN}}, \omega)$ , which has been confirmed by the deduced result of the normal (anomalous) self-energy based on the machine learning approach<sup>17</sup>. Moreover, this anticipated peak energy  $\omega_{\text{Im-Th}} \sim -70$  meV in the optimal doping is also qualitatively consistent with the corresponding result<sup>17</sup> of  $\omega_{\text{Im-ML}} \sim -65$  meV deduced in the optimally doped  $\text{Bi}_2\text{Sr}_2\text{CaCu}_2\text{O}_{8+\delta}$  via machine learning.

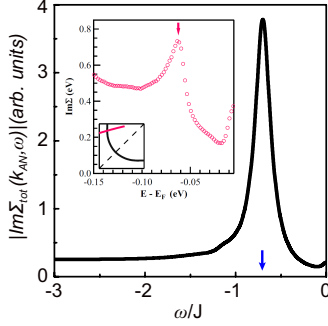


FIG. 3: (Color online) The imaginary part of the total self-energy at the antinode as a function of energy in  $\delta = 0.15$  with  $T = 0.002J$  for  $t/J = 3.5$  and  $t'/t = 0.4$ , where the blue arrow indicates the position of the peak. Inset: the corresponding experimental result of the optimally doped  $\text{Bi}_2\text{Sr}_2\text{CaCu}_2\text{O}_{8+\delta}$  taken from Ref. 27.

In the SC-state, although the normal and anomalous self-energies describe theoretically different parts of the interaction effects, all of them make the contributions to the dramatic change in the spectral line-shape of the single-particle excitation spectrum. To see this point more clearly, we plot the imaginary part of the total self-energy  $\text{Im}\Sigma_{\text{tot}}(\mathbf{k}_{\text{AN}}, \omega)$  [then the quasiparticle scattering rate  $\Gamma(\mathbf{k}_{\text{AN}}, \omega) = -\text{Im}\Sigma_{\text{tot}}(\mathbf{k}_{\text{AN}}, \omega)$ ] at the antinode as a function of energy for  $\delta = 0.15$  with  $T = 0.002J$  in Fig. 3 in comparison with the corresponding experimental result<sup>27</sup> found in the optimally doped  $\text{Bi}_2\text{Sr}_2\text{CaCu}_2\text{O}_{8+\delta}$  around the antinode (inset). It should be noted that the well-pronounced peak-structure in  $\text{Im}\Sigma_{\text{tot}}(\mathbf{k}_{\text{AN}}, \omega)$  in Fig. 3 is inconsistent with the corresponding result<sup>17</sup> deduced from the optimally doped  $\text{Bi}_2\text{Sr}_2\text{CaCu}_2\text{O}_{8+\delta}$  via machine learning, where although the sharp peaks appear in both the normal and anomalous self-energies, they cancel in the imaginary part of the total self-energy to make the structure apparently invisible. However, this peak structure in  $\text{Im}\Sigma_{\text{tot}}(\mathbf{k}_{\text{AN}}, \omega)$  in Fig. 3 is very well consistent with the corresponding experimental result observed<sup>27</sup> in the optimally doped  $\text{Bi}_2\text{Sr}_2\text{CaCu}_2\text{O}_{8+\delta}$ . At the antinode,  $\text{Im}\Sigma_{\text{tot}}(\mathbf{k}_{\text{AN}}, \omega)$  reaches a sharp peak at the energy of  $-70$  meV, and then the weight of the peak decreases rapidly in both the low-energy and high-energy ranges. Concomitantly, this theoretical peak-energy of

$-70$  meV in the optimum doping is also in qualitatively agreement with the peak energy<sup>27</sup> of  $-62$  meV detected in the optimally doped  $\text{Bi}_2\text{Sr}_2\text{CaCu}_2\text{O}_{8+\delta}$ . More surprisingly, the position of this sharp peak in  $\text{Im}\Sigma_{\text{tot}}(\mathbf{k}_{\text{AN}}, \omega)$  is just corresponding to the position of the dip in the PDH structure in the single-particle excitation spectrum shown in Fig. 1b, and therefore the peak-structure in  $\text{Im}\Sigma_{\text{tot}}(\mathbf{k}_{\text{AN}}, \omega)$  induces an intensity depletion in the single-particle excitation spectrum around the dip<sup>29</sup>. In other words, the peak-structure in  $\text{Im}\Sigma_{\text{tot}}(\mathbf{k}_{\text{AN}}, \omega)$  in Fig. 3 is directly responsible for the famous PDH structure in the single-particle excitation spectrum shown in Fig. 1b. Moreover, it has been shown that this peak structure in  $\text{Im}\Sigma_{\text{tot}}(\mathbf{k}_{\text{AN}}, \omega)$  can persist into the normal-state<sup>29</sup>, leading to that the PDH structure is totally unrelated to superconductivity.

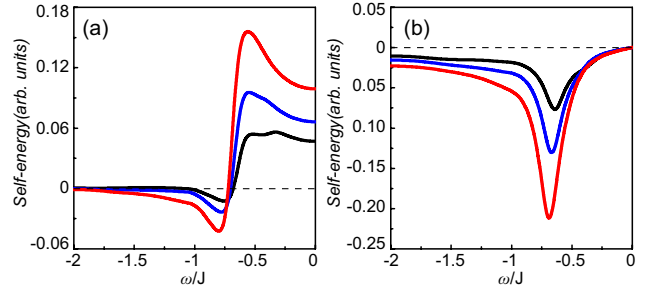


FIG. 4: (Color online) The (a) real and (b) imaginary parts of the anomalous self-energy at the antinode as a function of energy in  $\delta = 0.06$  (black line),  $\delta = 0.09$  (blue line), and  $\delta = 0.12$  (red line) with  $T = 0.002J$  for  $t/J = 3.5$  and  $t'/t = 0.4$ .

As a natural consequence of the doped Mott insulators, the normal and anomalous self energies in cuprate superconductors evolve with doping. In Fig. 4, we plot the results of the (a) real and (b) imaginary parts of the anomalous self-energy at the antinode as a function of energy for  $\delta = 0.06$  (black line),  $\delta = 0.09$  (blue line), and  $\delta = 0.12$  (red line) with  $T = 0.002J$ . It is thus shown clearly that in the underdoped regime, when the doping concentration is increased, (i) the peaks in both  $\text{Re}\Sigma_{\text{pp}}(\mathbf{k}_{\text{AN}}, \omega)$  and  $\text{Im}\Sigma_{\text{pp}}(\mathbf{k}_{\text{AN}}, \omega)$  move to higher energies, and (ii) the weights of these peaks are increased, which are nothing, but the SC gap that increases in magnitude with doping in the underdoped regime. Moreover, the evolution of the imaginary part of the normal self-energy with doping at around the  $[\pi, 0]$  point of BZ has been also investigated<sup>29</sup>, and results show that in the underdoped regime, the peak in  $\text{Im}\Sigma_{\text{ph}}(\mathbf{k}, \omega)|_{\mathbf{k}=[\pi, 0]}$  shifts to lower energies with the increase of doping, which leads to that both the hump and lowest-energy peak in the PDH structure of the single-particle excitation spectrum at around the  $[\pi, 0]$  point move to lower energies with the increase of doping, also in qualitative agreement with the corresponding ARPES experimental results<sup>25</sup>.

Now we turn to discuss the evolution of the normal and anomalous self-energies with momentum. In Fig. 5, we plot the real (blue line) and imaginary (red line) parts of

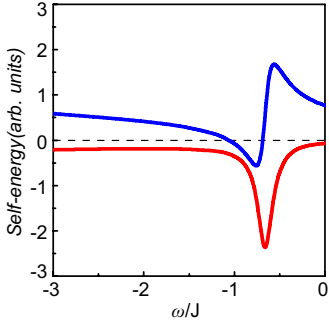


FIG. 5: (Color online) The real (blue line) and imaginary (red line) parts of the normal self-energy at the node as a function of energy in  $\delta = 0.15$  with  $T = 0.002J$  for  $t/J = 3.5$  and  $t'/t = 0.4$ .

the normal self-energy at the node as a function of energy for  $\delta = 0.15$  with  $T = 0.002J$ . In comparison with the corresponding result in Fig. 2a for the same set of parameters except for at the node, it is shown clearly when one moves the momentum  $\mathbf{k}_F$  from the antinode to the node, the weights of the peaks in both  $\text{Re}\Sigma_{\text{ph}}(\mathbf{k}_{\text{ND}}, \omega)$  and  $\text{Im}\Sigma_{\text{ph}}(\mathbf{k}_{\text{ND}}, \omega)$  are reduced, while the peaks move to lower energies. On the other hand, in the kinetic-energy driven SC mechanism<sup>19–22</sup>, the characteristic feature of the d-wave SC-state is the existence of four nodes on EFS, where the SC gap vanishes  $\Sigma_{\text{pp}}(\mathbf{k}_{\text{ND}}, \omega) = 0$ . Moreover, it has been found in the previous studies that the peak structures in both the normal and anomalous self-energies disappear at around the hot spots, where  $\Sigma_{\text{ph}}(\mathbf{k}_{\text{HS}}, \omega)$  and  $\Sigma_{\text{pp}}(\mathbf{k}_{\text{HS}}, \omega)$  have the anomalously small values, reflecting a fact that the coupling strength of the electrons to spin excitations is quite weak<sup>39</sup>.

At the temperature above  $T_c$ , the electrons are in a normal-state, where the SC gap  $\Sigma_{\text{pp}}(\mathbf{k}, \omega) = 0$ . However, the peak structure in the normal self-energy can persist into the normal-state. To see this point more clearly, we plot the results of the real (blue line) and imaginary (red line) parts of the normal self-energy at (a) the antinode and (b) the node as a function of energy for  $\delta = 0.15$  with  $T = 0.15J$  in Fig. 6. In comparison with the corresponding results in Fig. 2a and Fig. 5 for the same set of parameters except for in the normal-state ( $T = 0.15J$ ), one can find that although the weights of the peaks are suppressed with the increase of temperatures, the positions of these peaks in the normal-state do not change much from the corresponding case in the SC-state. This is why some characteristic features in the single-particle excitation spectrum of cuprate superconductors arising from the renormalization of the electrons can be detected from experiments in both the SC-state and normal-state.

To examine a microscopic SC theory, it should be to compare the normal and anomalous self-energies rather than the total self-energy. In the kinetic-energy driven SC mechanism<sup>19–22</sup>, the exchanged spin excitations give rise to the peak-structures both in the normal self-energy  $\Sigma_{\text{ph}}(\mathbf{k}, \omega)$  and anomalous self-energy  $\Sigma_{\text{pp}}(\mathbf{k}, \omega)$ . The

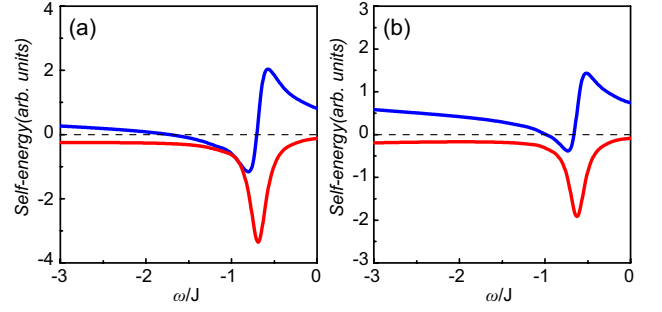


FIG. 6: (Color online) The real (blue line) and imaginary (red line) parts of the normal self-energy at (a) the antinode and (b) the node as a function of energy in  $\delta = 0.15$  with  $T = 0.15J$  for  $t/J = 3.5$  and  $t'/t = 0.4$ .

qualitative agreement between the peak-structures in the normal and anomalous self-energies obtained based on the kinetic-energy driven superconductivity and those deduced from the ARPES spectra of cuprate superconductors via machine learning<sup>17</sup> therefore shows why the theory of the kinetic-energy driven superconductivity can give a consistent description of the renormalization of the electrons in cuprate superconductors.

In conclusion, we have compared the results of the normal and anomalous self-energies deduced from the ARPES spectra of cuprate superconductors via machine learning with these obtained based on the kinetic-energy driven superconductivity, and the results show that both the normal and anomalous self-energies due to the interaction between electrons mediated by spin excitations exhibit the well-pronounced peak-structures at all around EFS except for at the hot spots, where the peak-structures are predicted to be absent. In particular, the peak-structure in the normal self-energy is mainly responsible for the PDH structure in the single-particle excitation spectrum, and can persist into the normal-state, while the sharp peak in the anomalous self-energy gives rise to a crucial contribution to the SC gap, and vanishes in the normal-state. Furthermore, these peak-structures in both the normal and anomalous self-energies evolve with doping, with the peak in the anomalous self-energy at around the antinode region that moves to higher energies as the doping concentration is increased in the underdoped regime. More specifically, these peaks have a special momentum dependence, where although the weight of the peak in the normal self-energy is gradually reduced when one moves the momentum from antinode to node, the position of the peak moves to lower energies.

## Acknowledgements

This work was supported by the National Key Research and Development Program of China under Grant No. 2016YFA0300304, and the National Natural Science Foundation of China under Grant Nos. 11974051 and

11734002.

- <sup>1</sup> J. G. Bednorz and K. A. Müller, Z. Phys. B **64**, 189 (1986).
- <sup>2</sup> P. W. Anderson, Science **235**, 1196 (1987).
- <sup>3</sup> See, e.g., the review, A. Damascelli, Z. Hussain, and Z.-X. Shen, Rev. Mod. Phys. **75**, 473 (2003).
- <sup>4</sup> See, e.g., the review, J. C. Campuzano, M. R. Norman, M. Randeria, in *Physics of Superconductors*, vol. II, edited by K. H. Bennemann and J. B. Ketterson (Springer, Berlin Heidelberg New York, 2004), p. 167.
- <sup>5</sup> See, e.g., the review, Joerg Fink, Sergey Borisenko, Alexander Kordyuk, Andreas Koitzsch, Jochen Geck, Volodymyr Zabolotnyy, Martin Knupfer, Bernd Buechner, and Helmut Berger, in *Lecture Notes in Physics*, vol. 715, edited by Stefan Hufner (Springer-Verlag Berlin Heidelberg, 2007), p. 295.
- <sup>6</sup> See, e.g., the review, Jules P. Carbotte, Thomas Timusk, and Jungseok Hwang, Rep. Prog. Phys. **74**, 066501 (2011).
- <sup>7</sup> Jin Mo Bok, Jong Ju Bae, Han-Yong Choi, Chandra M. Varma, W. Zhang, J. He, Y. Zhang, L. Yu, and X. J. Zhou, Sci. Adv. **2**, e1501329 (2016).
- <sup>8</sup> J. Bardeen, L. N. Cooper, and J. R. Schrieffer, Phys. Rev. **108**, 1175 (1957).
- <sup>9</sup> G. M. Eliashberg, Sov. Phys. JETP **11**, 696 (1960).
- <sup>10</sup> D. J. Scalapino, J. R. Schrieffer, and J. W. Wilkins, Phys. Rev. **148**, 263 (1966).
- <sup>11</sup> L. P. Gorkov, Sov. Phys. JETP **34**, 505 (1958).
- <sup>12</sup> Y. Nambu, Phys. Rev. **117**, 648 (1960).
- <sup>13</sup> See, e.g., the review, Tom Timusk and Bryan Statt, Rep. Prog. Phys. **62**, 61 (1999).
- <sup>14</sup> See, e.g., the review, S. Hufner, M. A. Hossain, A. Damascelli, and G. A. Sawatzky, Rep. Prog. Phys. **71**, 062501 (2008).
- <sup>15</sup> See, e.g., the review, Riccardo Comin and Andrea Damascelli, Annu. Rev. Condens. Matter Phys. **7**, 369 (2016).
- <sup>16</sup> See, e.g., the review, I. M. Vishik, Rep. Prog. Phys. **81**, 062501 (2018).
- <sup>17</sup> Youhei Yamaji, Teppei Yoshida, Atsushi Fujimori, and Masatoshi Imada, arXiv:1903.08060.
- <sup>18</sup> Andrey V. Chubukov and Jörg Schmalian, arXiv:2002.02994.
- <sup>19</sup> Shiping Feng, Phys. Rev. B **68**, 184501 (2003); Shiping Feng, Tianxing Ma, and Huaiming Guo, Physica C **436**, 14 (2006).
- <sup>20</sup> Shiping Feng, Huaisong Zhao, and Zheyu Huang, Phys. Rev. B **85**, 054509 (2012); Phys. Rev. B **85**, 099902(E) (2012).
- <sup>21</sup> See, e.g., the review, Shiping Feng, Yu Lan, Huaisong Zhao, Lulin Kuang, Ling Qin, and Xixiao Ma, Int. J. Mod. Phys. B **29**, 1530009 (2015).
- <sup>22</sup> Shiping Feng, Lulin Kuang, and Huaisong Zhao, Physica C **517**, 5 (2015).
- <sup>23</sup> D. S. Dessau, B. O. Wells, Z.-X. Shen, W. E. Spicer, A. J. Arko, R. S. List, D. B. Mitzi, and A. Kapitulnik, Phys. Rev. Lett. **66**, 2160 (1991).
- <sup>24</sup> M. R. Norman, H. Ding, J. C. Campuzano, T. Takeuchi, M. Randeria, T. Yokoya, T. Takahashi, T. Mochiku, and K. Kadowaki, Phys. Rev. Lett. **79**, 3506 (1997).
- <sup>25</sup> J. C. Campuzano, H. Ding, M. R. Norman, H. M. Fretwell, M. Randeria, A. Kaminski, J. Mesot, T. Takeuchi, T. Sato, T. Yokoya, T. Takahashi, T. Mochiku, K. Kadowaki, P. Guptasarma, D. G. Hinks, Z. Konstantinovic, Z. Z. Li, and H. Raffy, Phys. Rev. Lett. **83**, 3709 (1999).
- <sup>26</sup> J. Wei, Y. Zhang, H. W. Ou, B. P. Xie, D. W. Shen, J. F. Zhao, L. X. Yang, M. Arita, K. Shimada, H. Namatame, M. Taniguchi, Y. Yoshida, H. Eisaki, and D. L. Feng, Phys. Rev. Lett. **101**, 097005 (2008).
- <sup>27</sup> Daixiang Mou, Adam Kaminski, and Genda Gu, Phys. Rev. B **95**, 174501 (2017).
- <sup>28</sup> Deheng Gao, Yiqun Liu, Huaisong Zhao, Yingping Mou, and Shiping Feng, Physica C **551**, 72 (2018).
- <sup>29</sup> Deheng Gao, Yingping Mou, and Shiping Feng, J. Low Temp. Phys. **192**, 19 (2018).
- <sup>30</sup> Deheng Gao, Yingping Mou, Yiqun Liu, Shuning Tan, and Shiping Feng, Phil. Mag. **99**, 752 (2019).
- <sup>31</sup> M. R. Norman, H. Ding, M. Randeria, J. C. Campuzano, T. Yokoya, T. Takeuchi, T. Takahashi, T. Mochiku, K. Kadowaki, P. Guptasarma, and D. G. Hinks, Nature **392**, 157 (1998).
- <sup>32</sup> A. Kanigel, M. R. Norman, M. Randeria, U. Chatterjee, S. Souma, A. Kaminski, H. M. Fretwell, S. Rosenkranz, M. Shi, T. Sato, T. Takahashi, Z. Z. Li, H. Raffy, K. Kadowaki, D. Hinks, L. Ozyuzer, and J. C. Campuzano, Nature Phys. **2**, 447 (2006).
- <sup>33</sup> T. Yoshida, X. J. Zhou, K. Tanaka, W. L. Yang, Z. Hussain, Z.-X. Shen, A. Fujimori, S. Sahrakorpi, M. Lindroos, R. S. Markiewicz, A. Bansil, Seiki Komiya, Yoichi Ando, H. Eisaki, T. Kakeshita, and S. Uchida, Phys. Rev. B **74**, 224510 (2006).
- <sup>34</sup> Takeshi Kondo, Ari D. Palczewski, Yoichiro Hamaya, Tsunehiro Takeuchi, J. S. Wen, Z. J. Xu, Genda Gu, and Adam Kaminski, Phys. Rev. Lett. **111**, 157003 (2013).
- <sup>35</sup> B. Loret, Y. Gallais, M. Cazayous, R. D. Zhong, J. Schneeloch, G. D. Gu, A. Fedorov, T. K. Kim, S. V. Borisenko, and A. Sacuto, Phys. Rev. B **97**, 174521 (2018).
- <sup>36</sup> U. Chatterjee, M. Shi, A. Kaminski, A. Kanigel, H. M. Fretwell, K. Terashima, T. Takahashi, S. Rosenkranz, Z. Z. Li, H. Raffy, A. Santander-Syro, K. Kadowaki, M. R. Norman, M. Randeria, and J. C. Campuzano, Phys. Rev. Lett. **96**, 107006 (2006).
- <sup>37</sup> Yang He, Yi Yin, M. Zech, Anjan Soumyanarayanan, Michael M. Yee, Tess Williams, M. C. Boyer, Kamallesh Chatterjee, W. D. Wise, I. Zeljkovic, Takeshi Kondo, T. Takeuchi, H. Ikuta, Peter Mistark, Robert S. Markiewicz, Arun Bansil, Subir Sachdev, E. W. Hudson, and J. E. Hoffman, Science **344**, 608 (2014).
- <sup>38</sup> Y. Sassa, M. Radović, M. Månsson, E. Razzoli, X. Y. Cui, S. Pailhès, S. Guerrero, M. Shi, P. R. Willmott, F. Miletto Granozio, J. Mesot, M. R. Norman and L. Patthey, Phys. Rev. B **83**, 140511(R) (2011).
- <sup>39</sup> Yingping Mou, Yiqun Liu, Shuning Tan, and Shiping Feng, Phil. Mag. **99**, 2718 (2019).